Towards a microscopic approach to the intermolecular interaction in solid C_{60}

S. Savin and A. B. Harris
Department of Physics, University of Pennsylvania, Philadelphia, Pennsylvania 19104-6369

T. Yildirim
University of Maryland, College Park, Maryland 20742
and National Institute of Standards and Technology, Gaithersburg, Maryland 20899

(Received 24 May 1996)

Although the calculation of the ground-state and thermodynamic properties of solid C_{60} have been the subject of intense research, our understanding is still based on *ad hoc* models that treat phenomenologically both the Coulomb and short-range part of the interaction potential between C_{60} molecules. These potentials do not predict well those properties not fitted to fix the free parameters of the model, and they also do not properly represent the Coulomb interaction between molecules. To remedy this situation, here we introduce a semiempirical model in which the Coulomb interaction is treated microscopically using the local-density approximation C_{60} molecular charge densities, and the short-range part of the potential is modeled phenomenologically via Lennard-Jones (LJ) 12-6 interactions between the centers, delocalized over the surfaces of C_{60} molecules. The regular LJ parameters σ and ϵ as well as multipole moments of the interaction centers distribution were taken to reproduce the details of the observed low-temperature structure. We found that the Coulomb interaction is dominated by the charge overlap between the neighboring C_{60} molecules, and is much larger than the interaction calculated using the multipole expansion of the charge densities. Contrary to common belief, this Coulomb interaction by itself does not lead to the observed low-temperature structure. However, combined with the proposed short-range interaction, it stabilizes $Pa\bar{3}$ spatial structure with the correct setting angle. We make a comprehensive comparison between the wide range of experimental results and predictions of our, as well as previously proposed models. Our results show that the proposed model has the best overall agreement with the experimental observations in both the low- and high-temperature phases. [S0163-1829(97)00422-0]

I. INTRODUCTION

The construction of a reliable potential for the interaction of C_{60} molecules is an important, long-standing problem. Shortly after the discovery of the orientational ordering transition in solid C_{60},[1] Cheng and Klein[2] proposed to describe the intermolecular potential as a sum of Lennard-Jones 12-6 interactions between carbon atoms on different molecules. However, soon it was found[3,4] that the lowest energy crystal configuration predicted by this model did not have the symmetry observed in experiments.

Lu *et al.*[5] and Sprik *et al.*[6] have proposed two similar ways to improve the performance of this model. They suggested to augment the Lennard-Jones potential with Coulomb interactions of charges placed on ''5-6'' (''single'') and ''6-6'' (''double'') bonds or on carbon sites. This ''second generation'' of the intermolecular potentials, constructed to reproduce the experimentally observed low-temperature structure, was not successful in explaining most of the other experimental results.[7] In addition, these models are open to criticism on the theoretical grounds. In particular, Yildirim *et al.*[8] have shown that the *ad hoc* charge distributions, proposed in these models, do not agree with local-density approximation (LDA) C_{60} molecular charge densities. Also, Lamoen and Michel[9] have pointed out that since a significant part of the molecular charge density is spread along intercarbon bonds, a realistic model for the intermolecular potential should include Lennard-Jones interaction centers placed on bonds in addition to carbons. In a series of papers Michel and co-workers[9–11] have introduced a multiparametric model which reproduces some of the experimental results obtained at room temperature. At the same time, no attempts were made to account for the experimental observations in the low-temperature phase. As we will show, the orientational part of Michel's potential does not reproduce very well the experimental observations in the simple cubic phase.

In addition to these *ad hoc* models, there were several studies of the intermolecular interactions based on *ab initio* techniques.[12,13] However, in these papers the computations were performed for C_{60} molecules, placed in the specific orientations, so that no information on the orientational dependence of the intermolecular interaction potentials was obtained. The complete LDA analysis of the intermolecular interactions is a very complicated task, requiring the self-consistent treatment of a cluster of C_{60} molecules. Some simplifying approaches are necessary to effectively deal with this problem. One of them, the Gordon-Kim statistical approach, uses the sum of the LDA charge densities of the isolated molecules as an approximation for the charge density in the solid. This approach, successfully utilized for carbon in graphite,[14] was applied to solid C_{60} by La Rocca[15] and Yildirim.[16] While the values of the lattice constant, cohesive energy, and bulk modulus calculated within this approach[15] were in reasonable agreement with the experimental ones, the predicted details of the orientational ordering in the low-temperature phase were not.[15,16] This result

can be attributed to the fact that the Gordon-Kim approach is not successful in dealing with the short-range part of the intermolecular interaction (SRI). However, as was shown in Ref. 16, this approach is very useful in studying the Coulomb part of the interaction, which was found to be dominated by the charge overlap between neighboring molecules and to be of crucial importance for the stabilization of the $Pa3$ structure at low temperatures.

The demonstrated importance of the microscopic treatment of the Coulomb interaction between molecules (Refs. 8,16) as well as the necessity to find a good compromise between simple ''Lennard-Jones carbon-carbon''[5,6] and complete LDA approaches to the SRI motivated us to develop a new model for the intermolecular potential. In the present paper we use the previously determined molecular LDA charge densities to compute the Coulomb part of the intermolecular interaction. The SRI is represented by the Lennard-Jones 12-6 potential, acting between the centers distributed over the surface of the carbon cage. The characteristics of the Lennard-Jones potential as well as the multipole moments of the interacting centers distribution were used as adjustable parameters. This phenomenological approach to the SRI is a reasonable alternative to the complete cluster LDA calculation mentioned above. As a result we obtain a potential which, on the one hand, uses the molecular charge density obtained from a quantum-chemical calculation, and, on the other hand, has the best overall performance with respect to the experimental observations.

The present paper is organized as follows. In Sec. II we discuss some of the experimental results obtained for solid C_{60} and their interpretation in terms of the intermolecular potential. Section III deals with general theoretical framework used to describe the intermolecular interactions. There we introduce our model and discuss the choice of the adjustable parameters we have made. In Sec. IV we present the mean-field stability analysis of our potential and compute the values of the local orientational order parameters at room temperature. We also present the values of the libron frequencies predicted by our model. These results are compared with the experimental data as well as with the predictions from other potentials. Section V summarizes our conclusions. Finally, in the Appendixes we present some of the technical details of our calculations.

II. EXPERIMENTAL OBSERVATIONS IN C_{60} SOLIDS AND THE INTERMOLECULAR INTERACTION POTENTIAL

At $T \approx 260$ K solid C_{60} undergoes a first-order phase transition in which the icosahedral [point group I_h (Ref. 17)] molecules develop long-range orientational order.[1] In both the high-temperature orientationally disordered phase (space group $Fm\bar{3}m$) and the orientationally ordered phase (space group $Pa3$) the molecular centers of mass form an fcc lattice. The molecular orientations in the $Pa3$ phase are obtained as follows. Consider a fiducial state in which all molecules are in standard orientation A as shown in Fig. 1. Then each molecule is rotated through a setting angle ϕ about the local threefold axis.[18,19] This structure has been confirmed by additional diffraction measurements.[20,21]

Subsequent to the initial observation of the phase transition, solid C_{60} was the object of extensive study by various experimental techniques. Much of this body of evidence can be related to the specific features of the intermolecular interaction and thus serves to set requirements which ought to be satisfied by any prospective model. This section discusses some of the major experimental findings and their connection to the intermolecular potential.

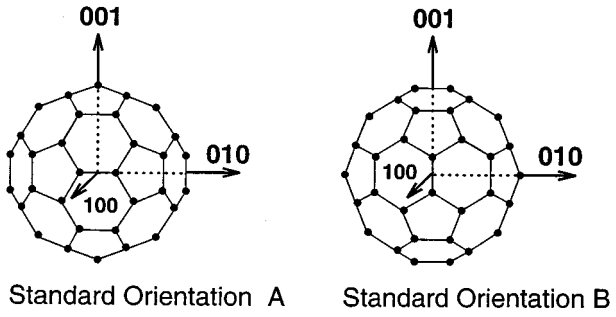

FIG. 1. C_{60} molecule in standard orientations A and B with respect to the crystal axes.

One of the important studies of the local orientational order in the low-temperature phase of solid C_{60} was performed by David and co-workers.[21–23] By analyzing the temperature evolution of the high-resolution neutron powder-diffraction profile, this group has confirmed the low-temperature value of simple cubic lattice constant $a = 14.04$ Å, measured by Heiney *et al.*[1] David *et al.* also suggested that at very low temperatures the orientation of the majority of C_{60} molecules is described by the setting angle of $\approx 22°$, while the minority finds itself in the orientation with the setting angle of about 82°. The energy difference between these two orientations was found to be 11 meV,[23] a value, confirmed later by Yu *et al.*[24] Therefore, we require that for an intermolecular potential to be acceptable, the $Pa3$ configuration with a setting angle of about 22° should correspond to the global minimum in the potential energy of the crystal. At the same time, changing the setting angle of one molecule from its global minimum value to the value around 82° should bring the crystal into a configuration corresponding to the local minimum of its potential energy—and the energy difference between these minima should be equal to 11 meV. In addition, the equilibrium separation between the molecules in the $Pa3$ global minimum configuration should correspond to the experimentally obtained value of the low-temperature lattice constant.

Another feature of the intermolecular potential is usually associated with the phenomenon of orientational freezing observed at $T \approx 90$ K. The results obtained via various experimental techniques[24–28] consistently point to the existence of an energetic barrier of 235–280 meV between the global minimum and the local minimum orientations of the molecule in $Pa3$ phase.

The experimental value of the low-temperature bulk modulus can be related to the second derivative of the potential energy of the crystal in the global minimum $Pa3$ configuration with respect to the lattice constant at the equilibrium separation. Ludwig *et al.*[29] have obtained the values of 14.7 and 14.2 GPa for the bulk modulus in the simple cubic phase[29] at 70 and 170 K, respectively. At the same

TABLE I. The experimental results interpreted in terms of the properties of the intermolecular interaction potential. The corresponding references are given in parentheses.

Experimental quantity	Measured value
Setting angles of the global and local minima configurations in $Pa\bar{3}$	22°, 82° (Ref. 21)
The energy difference between the minima	11 meV (Ref. 21)
The energy barrier between the minima	235–290 meV (Refs. 24–28)
Lattice constant at $T\approx 0$	14.04 Å (Ref. 21)
Bulk modulus at low temperature	14.7 GPa (Ref. 29) 10.3 GPa (Ref. 30)
Cohesive energy	-1.6 eV (Ref. 32), -1.7 eV (Ref. 33), -1.74 eV (Ref. 34)
Orientational order parameters:	
γ_6	-0.386 -0.395
γ_{10}	0.217 0.359
γ_{12}^1	0.159 0.228
γ_{12}^2	0.440 (Ref. 36), 0.0706 (Ref. 11)
Libron frequencies at $q\approx 0$	2.2–6.2 meV (Refs. 40,41)

time, Lundin and Sundqvist[30] have reported the much lower value of 10.3 GPa from measurements at 152 K. In addition, different groups report rather different results for the measurements of the bulk modulus at room temperature, e.g., 13.4 GPa,[29] 6.7 GPa,[30] 14.2 GPa.[31] It is clear that some additional experiments are necessary to establish the reason for the above-mentioned discrepancy.

The experimental value of cohesive energy can be associated with the value of the potential energy at equilibrium. The measurements of the cohesive energy by Kataura *et al.*,[32] Pan *et al.*,[33] and Abrefah *et al.*[34] yielded the values of E_0 to be -1.7, -1.74, -1.65 eV/molecule, respectively.

The important information on the shape of the orientational potential in the high-temperature phase is provided by the values of the local orientational order parameters γ_l^μ. These order parameters (which are dimensionless) are related to the thermal averages $\langle U_{l,\mu}\rangle$ of the so-called molecular rotator functions $U_{l,\mu}(\alpha,\beta,\gamma)$:[35]

$$\gamma_l^\mu = \kappa_l \langle U_{l,\mu}\rangle, \tag{1}$$

where κ_l are the multipole moments of the carbon atoms distribution on the surface of the molecular cage. Above the orientational ordering transition temperature the only nonzero values of γ_l^μ are those belonging to A_{1g} representations of the O_h group, $\gamma_l^\mu = \gamma_l^\rho \delta_{\mu,(\rho 1)}$. The values of γ_l^ρ were measured at room temperature using x-ray synchrotron and neutron powder-diffraction techniques.[11,36] The obtained order parameters for $l=6,10,12$ are presented in Table I: two values for $l=12$ correspond to two different irreducible representations of A_{1g} symmetry. As one can see, the values for γ_6, γ_{10}, and γ_{12}^1 coming from these two experiments, agree with each other quite well and therefore are probably more reliable than the value for γ_{12}^2.

The comparison between computed libron frequencies and the experimentally measured ones can serve as yet another test for the orientational part of the interaction potential. The librational phonon modes in C_{60} single crystals were studied most extensively by Pintschovius and co-workers[37–39] and Horoyski.[40,41] The former group has performed several studies of the phonon-dispersion curves in C_{60} single crystals using inelastic neutron scattering. The initial assignment of the observed modes[37] was corrected in the later papers.[38,39] Their measurements at $T\approx 80$ K show the zone center librational modes at the approximate energies 2.2, 2.6, 3, and 4.3 meV. Horoyski *et al.* have used Fourier-transform Raman spectroscopy to perform high-resolution measurements of $q\approx 0$ libron frequencies. The experiments were performed at 77 K, and the Raman peaks were observed at 2.23, 2.61, 3.06, 4.07, 5.16, and 6.20 meV. However, one has to exercise caution in assigning the highest energy peaks reported there to single librons rather than to ''multilibrons.'' Another important feature to keep in mind is the ''stiffening'' libron spectrum undergoes when the temperature is lowered. Since the comparison between the computed and measured librational frequencies is most direct for experimental values taken at $T\approx 0$, one has to allow for possible corrections. In particular, the lowest energy peak[40,41] shifts only slightly to 2.3 meV when the temperature is lowered from 77 to 10 K. At the same time, the second peak[39] shifts to ≈ 2.8 meV, and from extrapolation one can expect comparable shifts for higher peaks as well.

TABLE II. The values of the expansion coefficients $a_{l,n}$ for the SARF of the icosahedral symmetry ($a_{0,0}=1$).

l	$n=0$	$n=\pm2$	$n=\pm4$	$n=\pm6$	$n=\pm8$	$n=\pm10$	$n=\pm12$
6	−0.207	0.475	0.388	−0.320			
10	0.354	0.288	−0.357	0.056	−0.425	−0.207	
12	−0.414	0.118	−0.183	−0.463	−0.074	0.292	−0.247

At the same time, the experimentally observed frequencies of the translational phonon modes[39] were shown to have largely fcc-type dispersion, so that their values can be adequately explained using only the values of the lattice constant and bulk modulus. Accordingly, in this paper we only concentrate on the libron frequencies. The experimental findings mentioned above are summarized in Table I.

III. SEMI-EMPIRICAL APPROACH TO THE INTERMOLECULAR INTERACTION IN SOLID C_{60}

The experimental results, described in the previous section, impose numerous restrictions on theoretical models for the intermolecular interaction of fullerenes. Unfortunately, none of the interaction potential models proposed so far performs well against all these experimental benchmarks—the further analysis is given in Sec. IV. To correct this situation, we propose a model for the intermolecular interactions which combines the microscopic treatment of the Coulomb interaction between molecules with the phenomenological approach to describing the short-range part of the potential. In this section we present the general theoretical framework we use, as well as details of our approach.

A. The general expressions for the interaction of two C_{60} molecules

Let us consider two molecules of icosahedral symmetry, interacting with each other in a crystal via a generalized inverse power potential with the exponent n (e.g., for the Coulomb interaction $n=1$ and for the Lennard-Jones 12-6 potential there will be expressions with $n=6$ and $n=12$). For simplicity we do not consider an exponential form of interaction, though similar expressions can be obtained for this case as well. Suppose that the positions of the molecular centers of mass are given by vectors $\mathbf{d}_1$ and $\mathbf{d}_2$ with respect to some fixed set of axes, for example, the one connected to the crystal. Let us also assume that with respect to the same set of axes the orientations of the molecules are described by Euler angles $\boldsymbol{\omega}_1=(\alpha_1,\beta_1,\gamma_1)$ and $\boldsymbol{\omega}_2$, respectively [(0,0,0) being standard orientation A]. Then the expression for the energy of interaction will be a linear combination of the contributions V_n, each of the form

$$V_n(\mathbf{d}_1,\boldsymbol{\omega}_1,\mathbf{d}_2,\boldsymbol{\omega}_2)=\int\int d\mathbf{r}_1 d\mathbf{r}_2 \frac{\rho_{\boldsymbol{\omega}_1}(\mathbf{r}_1)\rho_{\boldsymbol{\omega}_2}(\mathbf{r}_2)}{|\mathbf{r}_1-\mathbf{r}_2+\mathbf{d}_{12}|^n}, \quad (2)$$

where $\mathbf{d}_{12}=\mathbf{d}_1-\mathbf{d}_2$, and $\rho_{\boldsymbol{\omega}}(\mathbf{r})$ is the interaction center density. In particular, in the case of the Lennard-Jones atom-atom interaction this function is usually expressed as a sum of δ functions centered at the atomic sites. However, in general it can have different forms, with the icosahedral symmetry of the resulting expression being the only imposed requirement. We would like to emphasize that in solids because of the crystal-field effects the symmetry of C_{60} molecules is, strictly speaking, reduced from I_h to S_6. However, this distortion is small and will be neglected in further analysis. The interaction center density function can also be expressed as $\rho_{\boldsymbol{\omega}}(\mathbf{r})=\rho(\hat{R}^{-1}(\boldsymbol{\omega})\mathbf{r})$, where $\rho(\mathbf{r})$ is the interaction center density of C_{60} molecule in standard orientation A (see Fig. 1), and $\hat{R}(\boldsymbol{\omega})$ is the rotation described by three Euler angles $\boldsymbol{\omega}=(\alpha,\beta,\gamma)$. The function $\rho(\mathbf{r})$ transforms into itself under any operation of the icosahedral group I_h. Therefore,

$$\rho(\mathbf{r})=\rho(r,\hat{\mathbf{r}})=\sum_l \rho_l(r)T_l^{A_{1g}}(\hat{\mathbf{r}})=\sum_l \sum_{n=-l}^{l} a_{ln}\rho_l(r)Y_{ln}(\hat{\mathbf{r}}), \quad (3)$$

where $T_l^{A_{1g}}$ are the symmetry-adapted rotator functions (SARF)—the linear combinations of the spherical harmonics of order l belonging to the A_{1g} representation of the icosahedral group. SARF were introduced by James and Keenan[35] for the analysis of the orientational ordering in solid methane. Michel *et al.*[42] have applied them to the case of solid C_{60}. The sum in Eq. (3) runs over $l=0,6,10,12,16,18\ldots$, the values allowed by the molecular symmetry. In standard orientation A the values of the nonzero coefficients for $l=6,10,12$ are listed in Table II ($a_{0,0}=1$).

The multipole density functions $\rho_l(r)$ describe the details of the radial distribution of the interaction centers. Then, for the rotated molecule we have

$$\rho_{\boldsymbol{\omega}}(\mathbf{r})=\sum_{ln} a_{ln}\rho_l(r)Y_{ln}(\hat{R}^{-1}(\boldsymbol{\omega})\hat{\mathbf{r}})$$

$$=\sum_{l,m,n} a_{ln}\rho_l(r)Y_{lm}(\hat{\mathbf{r}})D^l_{mn}(\boldsymbol{\omega}), \quad (4)$$

where $D^l_{mn}(\boldsymbol{\omega})$ is a well known Wigner matrix.[43] Substituting the last expression into Eq. (2), we get

$$V_n(\mathbf{d}_1,\boldsymbol{\omega}_1,\mathbf{d}_2,\boldsymbol{\omega}_2)=\sum_{l_1m_1n_1}\sum_{l_2m_2n_2}a_{l_1n_1}D^{l_1}_{m_1n_1}(\boldsymbol{\omega}_1)a_{l_2n_2}D^{l_2}_{m_2n_2}(\boldsymbol{\omega}_2)\int\int d\mathbf{r}_1d\mathbf{r}_2\frac{\rho_{l_1}(r_1)Y_{l_1m_1}(\hat{\mathbf{r}}_1)\rho_{l_2}(r_2)Y_{l_2m_2}(\hat{\mathbf{r}}_2)}{|\mathbf{r}_1-\mathbf{r}_2+\mathbf{d}_{12}|^n}$$

$$=\sum_{l_1m_1}\sum_{l_2m_2}S^{l_1}_{m_1}(\boldsymbol{\omega}_1)S^{l_2}_{m_2}(\boldsymbol{\omega}_2)Q^{l_1l_2}_{m_1m_2}(\mathbf{d}_{12}), \tag{5}$$

where

$$S^l_m(\boldsymbol{\omega})=\sum_{n=-l}^{l}a_{ln}D^l_{mn}(\boldsymbol{\omega}), \tag{6}$$

and

$$Q^{l_1l_2}_{m_1m_2}(\mathbf{d})=\int\int d\mathbf{r}_1d\mathbf{r}_2\frac{\rho_{l_1}(r_1)\rho_{l_2}(r_2)Y_{l_1m_1}(\hat{\mathbf{r}}_1)Y_{l_2m_2}(\hat{\mathbf{r}}_2)}{|\mathbf{r}_1-\mathbf{r}_2+\mathbf{d}|^n}. \tag{7}$$

Thus, the complete information about the interaction of two molecules is ''stored'' in the interaction matrix $Q^{l_1l_2}_{m_1m_2}(\mathbf{d})$. To make use of this general expression we will separately consider Coulomb and Lennard-Jones (LJ) 12-6 interactions.

B. The Coulomb interaction between C_{60} molecules

As we shall see, ''bond charge'' models[5,6] do not properly describe the Coulomb interaction between fullerenes.[8,16] In the present paper we have computed this interaction by using the C_{60} molecular charge densities obtained from *ab initio* electronic wave functions.[8] We emphasize, that due to the significant overlap between the charge densities on the neighboring molecules in solids, the Coulomb interaction does not reduce itself to multipole-multipole coupling. This circumstance has important implications for the intermolecular potential.[16] In particular, because of the mentioned overlap, there is a significant contribution to the crystal-field potential, coming from the Coulomb interaction. Such a contribution involving a monopole is absent in the multipole expansion and has not been considered previously. For each molecule the Coulomb charge density naturally separates into core ($+4|e|$ per carbon site) and valence parts. The core charge density is given by

$$\rho^{\rm core}(\mathbf{r})=4|e|\sum_{k=1}^{60}\delta(\mathbf{r}-\mathbf{r}_k)$$

$$=4|e|\frac{\delta(r-R_0)}{R_0^2}\sum_{l=0,6\ldots}\kappa_lT_l^{A_1g}(\hat{\mathbf{r}}), \tag{8}$$

where $R_0=3.55$ Å is the molecular radius and the atomic multipole moments κ_l are found from

$$\kappa_l=\int d\mathbf{r}T_l^{A_1g}(\hat{\mathbf{r}})\sum_{k=1}^{60}\delta(\mathbf{r}-\mathbf{r}_k)=\sum_{k=1}^{60}T_l^{A_1g}(\hat{\mathbf{r}}_k), \tag{9}$$

so that $\kappa_0=60/\sqrt{4\pi}=16.93$, $\kappa_6=2.56$, $\kappa_{10}=19.35$, $\kappa_{12}=7.89$. Then, the core charge multipole density functions can be expressed as $\rho_l^{\rm core}(r)=4|e|\kappa_l[\,\delta(r-R_0)/R_0^2]$.

The values of the valence multipole density functions $\rho_l^{\rm val}(r)$ were computed for 41 different values of r. The results for $l=0,6,10,12$ are presented in Table III and are shown in Fig. 2. The values of $\rho_l^{\rm val}(r)$ for $l=16,18,\ldots$ at any r were found to be much smaller than those of $\rho_l^{\rm val}(r)$ for $l=0$, 6, 10, and 12. So in what follows we limit ourselves to considering only contributions from $\rho_l^{\rm val}(r)$ with l up to 12.

The interaction matrix [which we denote as $R^{l_1l_2}_{m_1m_2}(\mathbf{d})$] for Coulomb interaction between core charges on one molecule and the total (core and valence) charges on the neighboring molecule can be computed using two-center expansion (see Appendix B):

$$R^{l_1l_2}_{m_1m_2}(\mathbf{d})=4\frac{|e|^2}{d}(-1)^{l_1}\left(\frac{R_0}{d}\right)^{l_1+l_2}\frac{q_{l_10}}{a_{l_10}}\kappa_{l_2}\left(\frac{(4\pi)^3}{(2l_1+1)(2l_2+1)[2(l_1+l_2)+1]}\right)^{1/2}C((l_1,0)(l_2,0)(l_1+l_2))$$

$$\times\frac{(2l_1+1)(2l_2+1)[2(l_1+l_2)-1]!!}{(2l_1+1)!!(2l_2+1)!!}C((l_1,m_1)(l_2,m_2)(l_1+l_2))Y_{l_1+l_2,m_1+m_2}(\hat{\mathbf{d}}). \tag{10}$$

Here q_{lm} are the values of the reduced multipole moments of the molecular charge distribution, tabulated in Ref. 8, $C((l_1,m_1)(l_2,m_2)(l_1+l_2))$ are the Clebsch-Gordan coefficients,[43] and $n!!$ is defined as $2^{n/2}\times(n/2)!$ or $n!/\{2^{(n-1)/2}\times[(n-1)/2]!\}$ for even and odd n, respectively. For the Coulomb potential energy of two molecules, in addition to $R^{l_1l_2}_{m_1m_2}(\mathbf{d})$ there will also be a term $R^{l_2l_1}_{m_2m_1}(\mathbf{d})$, coming from the interaction between the core charges of the second molecule and the ''total'' charge cloud of the first one. However, to avoid double counting of the Coulomb interaction between the core charges one has to subtract this core-core term, whose interaction matrix is denoted $A^{l_1l_2}_{m_1m_2}(\mathbf{d})$, from the final result. This term is given by

TABLE III. The computed values of the valence multipole density functions according to LDA (in the units of $-|e|/\text{a.u.}^3$) for $l=0,6,10,12$. All numbers have uncertainty in their last digit.

r, a.u.	$\rho_0(r)$	$\rho_6(r)$	$\rho_{10}(r)$	$\rho_{12}(r)$
1.786	0.0672	0.000629	0.00183	0.000164
2.321	0.364	0.0145	0.0616	0.0103
2.500	0.664	0.0345	0.151	0.0272
2.678	1.162	0.0734	0.321	0.0624
2.857	1.900	0.140	0.608	0.129
2.946	2.360	0.186	0.808	0.179
3.035	2.867	0.241	1.046	0.242
3.125	3.390	0.301	1.303	0.313
3.214	3.850	0.358	1.528	0.374
3.303	4.160	0.400	1.661	0.406
3.393	4.310	0.426	1.710	0.415
3.446	4.390	0.443	1.775	0.440
3.500	4.520	0.472	1.948	0.510
3.571	4.530	0.486	2.049	0.557
3.642	4.150	0.442	1.773	0.462
3.714	3.860	0.413	1.656	0.431
3.785	3.570	0.385	1.583	0.420
3.857	3.220	0.348	1.468	0.395
3.928	2.823	0.303	1.303	0.352
4.017	2.307	0.244	1.066	0.286
4.107	1.830	0.189	0.840	0.222
4.196	1.421	0.143	0.646	0.168
4.285	1.084	0.106	0.489	0.125
4.375	0.814	0.0763	0.363	0.0913
4.464	0.602	0.0540	0.265	0.0655
4.553	0.440	0.0374	0.189	0.0458
4.642	0.319	0.0255	0.133	0.0314
4.732	0.230	0.0171	0.0916	0.0210
4.821	0.166	0.0113	0.0627	0.0138
4.910	0.121	0.00751	0.0429	0.00897
5.000	0.0886	0.00499	0.0294	0.00578
5.124	0.0583	0.00286	0.0177	0.00312
5.249	0.0391	0.00169	0.0109	0.00169
5.357	0.0279	0.00111	0.00735	0.00101
5.464	0.0200	0.000749	0.00506	0.000614
5.571	0.0144	0.000516	0.00353	0.000379
5.678	0.0102	0.000361	0.00248	0.000238
5.785	0.00720	0.000254	0.00174	0.000152
5.892	0.00501	0.000179	0.00122	0.0000983
5.982	0.00367	0.000133	0.000904	0.0000694
6.071	0.00266	0.0000983	0.000665	0.0000494

$$A^{l_1 l_2}_{m_1 m_2}(\mathbf{d}) = 16\frac{|e|^2}{d}(-1)^{l_1}\left(\frac{R_0}{d}\right)^{l_1+l_2}\kappa_{l_1}\kappa_{l_2}\left(\frac{(4\pi)^3}{(2l_1+1)(2l_2+1)[2(l_1+l_2)+1]}\right)^{1/2} C((l_1,0)(l_2,0)(l_1+l_2))$$
$$\times\frac{(2l_1+1)(2l_2+1)[2(l_1+l_2)-1]!!}{(2l_1+1)!!(2l_2+1)!!} C((l_1,m_1)(l_2,m_2)(l_1+l_2))Y_{l_1+l_2,m_1+m_2}(\hat{\mathbf{d}}). \quad (11)$$

Now, let us consider the interaction between the valence electrons. At the experimentally observed separations between fullerenes in the crystal there is a significant overlap between the valence charge densities on the neighboring molecules. Therefore, the convenient two-center expansion is not applicable, and this part of the Coulomb interaction [denoted as $B^{l_1 l_2}_{m_1 m_2}(\mathbf{d})$] needs special treatment. Starting with

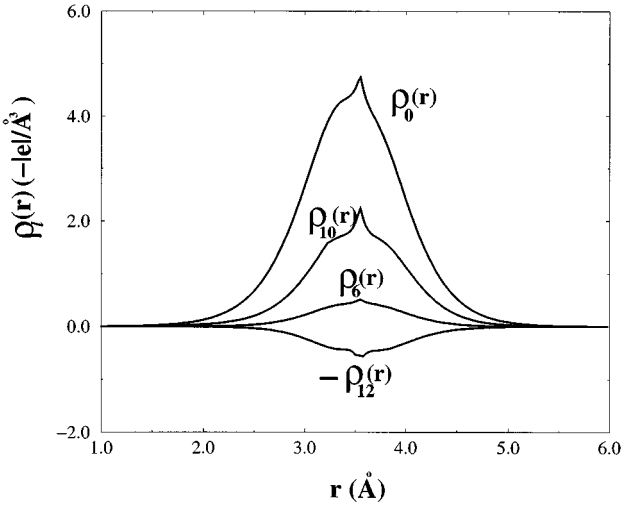

FIG. 2. The multipole charge density functions $\rho_l^{\rm val}(r)$, expressed in the units $-|e|/\text{Å}^3$ for $l=0,6,10,12$. The maximum around $r=3.55$ Å corresponds to the electrons localized near the carbon cage.

$$B^{l_1 l_2}_{m_1 m_2}(\mathbf{d}_{ij}) = \int\int d\mathbf{r}_1 d\mathbf{r}_2 \frac{\rho^{\rm val}_{l_1}(r_1)\rho^{\rm val}_{l_2}(r_2) Y_{l_1 m_1}(\hat{\mathbf{r}}_1) Y_{l_2 m_2}(\hat{\mathbf{r}}_2)}{|\mathbf{r}_1-\mathbf{r}_2+\mathbf{d}_{ij}|}, \tag{12}$$

and using the Fourier transform

$$\frac{1}{r} = \int \frac{d\mathbf{q}}{(2\pi)^3} e^{-i\mathbf{qr}} \frac{4\pi}{q^2}, \tag{13}$$

one gets

$$B^{l_1 l_2}_{m_1 m_2}(\mathbf{d}) = \int \frac{d\mathbf{q}}{(2\pi)^3} \frac{4\pi}{q^2} e^{-i\mathbf{qd}} I_{l_1 m_1}(-\mathbf{q}) I_{l_2 m_2}(\mathbf{q}), \tag{14}$$

where

$$I_{lm}(\mathbf{q}) = \int d\mathbf{r} \rho_l(r) e^{i\mathbf{qr}} Y_{lm}(\hat{\mathbf{r}}). \tag{15}$$

Now

$$e^{i\mathbf{qr}} = \frac{4\pi}{qr} \sum_{l=0}^{\infty} \sum_{m=-l}^{l} (i)^l j_l(qr) Y_{lm}(\hat{\mathbf{q}}) Y^*_{lm}(\hat{\mathbf{r}}), \tag{16}$$

where $j_l(x)=\sqrt{\pi x/2} J_{l+1/2}(x)$ is the spherical Bessel's function of order l. So,

$$I_{lm}(\mathbf{q}) = \frac{4\pi}{q}(i)^l Y_{lm}(\hat{\mathbf{q}}) \int_0^{\infty} r dr \rho_l(r) j_l(qr) \equiv \frac{4\pi}{q}(i)^l Y_{lm}(\hat{\mathbf{q}}) K_l(q). \tag{17}$$

Substituting the last expression into Eq. (14) and performing the integration over $d\hat{\mathbf{q}}$, one gets the final expression

$$B^{l_1 l_2}_{m_1 m_2}(\mathbf{d}) = \frac{32\pi}{d}(-1)^{l_1} \sum_{l_3=|l_1-l_2|}^{l_1+l_2} (i)^{l_1+l_2-l_3} \left(\frac{(2l_1+1)(2l_2+1)}{4\pi(2l_3+1)}\right)^{1/2} C[(l_1,m_1)(l_2,m_2)(l_3)] \times C[(l_1,0)(l_2,0)(l_3)] Y_{l_3, m_1+m_2}(\hat{\mathbf{d}}) \int_0^{\infty} \frac{dq}{q^3} K_{l_1}(q) K_{l_2}(q) j_{l_3}(qd). \tag{18}$$

This way one reduces the computation of $B^{l_1 l_2}_{m_1 m_2}(\mathbf{d})$ to calculating a number of one-dimensional integrals involving

$$K_l(q) = \int_0^{\infty} r dr \rho^{\rm val}_l(r) j_l(qr) \tag{19}$$

for $l=0,6,10,12$.

Thus, the total Coulomb interaction matrix, $D^{l_1 l_2}_{m_1 m_2}(\mathbf{d})$, can be written as

$$D^{l_1 l_2}_{m_1 m_2}(\mathbf{d}) = B^{l_1 l_2}_{m_1 m_2}(\mathbf{d}) + R^{l_1 l_2}_{m_1 m_2}(\mathbf{d}) + R^{l_2 l_1}_{m_2 m_1}(\mathbf{d}) - A^{l_1 l_2}_{m_1 m_2}(\mathbf{d}). \tag{20}$$

The resulting Coulomb interaction differs significantly from both the multipole-multipole interaction[8] and the Coulomb interactions from ''bond-charge'' models. To illustrate this point, we have computed the variation of the Coulomb potential energy with the setting angle in the $Pa\bar{3}$ phase for our model as well as for the multipole-multipole interaction and for the Coulomb interaction from the model of Lu *et al.*[5] (later referred to as the LLM model). The results are shown in Fig. 3. As one can see, these potentials are qualitatively different: while the LLM model predicts, that the Coulomb interaction has a local minimum at setting angle of $\approx 22°$ and a local maximum at $\approx 85°$, our microscopic model states that at both setting angles the total Coulomb interaction is maximized.[16] The unrealistic nature of the Coulomb part of the LLM model is clearly seen in the following observation. At both setting angles the molecular 6-6 (''double'') bonds face the centers of the ''pentagons'' (setting angle of $\approx 22°$) or ''hexagons'' (setting angle of $\approx 85°$) of their nearest neighbors. Since the charge densities are very similar for ''hexagons'' and ''pentagons,'' the interaction energy should be either maximized or minimized for both setting angles and definitely not maximized for one and minimized for the other. Another interesting conclusion comes from the analysis of the curve for the multipole-multipole interaction,[8] which was computed using the same LDA charge densities we used in the present work, however, neglecting the overlap

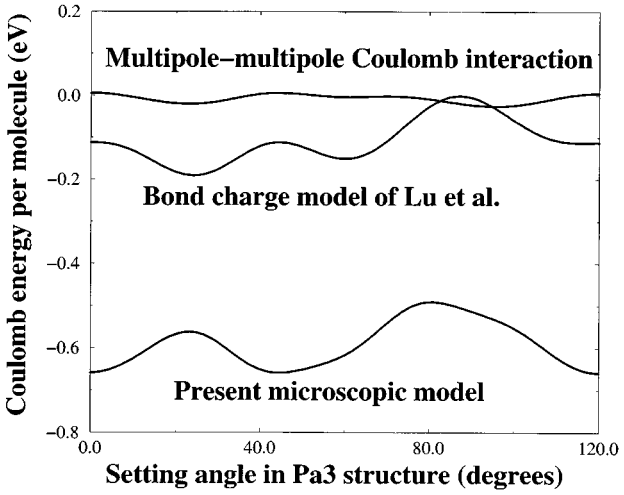

FIG. 3. The Coulomb potential energy per molecule as a function of the setting angle in the $Pa3$ phase for various models: (a) our model, (b) model of Lu *et al.*, (c) multipole interaction, computed by Yildirim *et al.*

between the charges on neighboring molecules. As we see, this approach leads to a significant underestimation of the magnitude of the Coulomb interaction. In addition, neglecting the charge overlap leads to the different orientational dependence of the Coulomb part of the potential energy.

These observations show that the widely accepted assumption about the intermolecular electrostatic interactions being minimized when the 6-6 bond on one molecule faces either pentagons or hexagons on the neighboring molecules,[22,44] is not supported by the microscopic calculation. In fact, the Coulomb interactions are maximized for these mutual orientations. However, as we will show in the next section, being combined with the proposed short-range part of the potential, the microscopic Coulomb interaction does lead to the stabilization of the $Pa3$ structure with the correct setting angle.

C. The short-range part of the intermolecular interaction

In the early models of the intermolecular potential in C_{60} solids[2,5,6] the SRI was represented by carbon-carbon LJ 12-6 interactions. This was an over-simplification, since it ignored the repulsion between charges on intercarbon bonds. Michel *et al.* have proposed to introduce additional interaction centers on 5-6 and 6-6 bonds in order to reach an agreement with the experiment on the values of the crystal-field coefficients.[9–11] However, as will be shown in Sec. IV, the performance of the orientational part of the potential with regard to the details of the low-temperature structure was still not satisfactory. At the same time, the Gordon-Kim approach attempted by La Rocca[15] and Yildirim[16] had not shown much of an improvement in this regard either. These results have persuaded us to search for the reliable intermediate approach to modeling SRI so as to avoid having to implement a full-scale LDA or to use the overly simplistic recipes of early models. In this paper we have developed a model where SRI comes from the LJ 12-6 interactions between the interaction centers densities, delocalized over the surface of the carbon cage, not necessarily exclusively over intercarbon bonds. Then, the interaction centers multipole density functions $\rho_l^i(r)$ can be expressed as

$$\rho_l^i(r)=\frac{\delta(r-R_0)}{R_0^2}\kappa_l^i, \tag{21}$$

where κ_l^i is the lth multipole of the interaction centers distribution over the surface of the molecule and R_0 is the molecular radius. Then, as in Eq. (5), SRI for the two molecules becomes

$$\begin{aligned}V_{\mathrm{LJ}}(\mathbf{d}_1,\boldsymbol{\omega}_1,\mathbf{d}_2,\boldsymbol{\omega}_2)=&\int\int d\mathbf{r}_1 d\mathbf{r}_2 4\epsilon\left(\frac{\sigma^{12}}{|\mathbf{r}_1-\mathbf{r}_2+\mathbf{d}_{12}|^{12}}-\frac{\sigma^6}{|\mathbf{r}_1-\mathbf{r}_2+\mathbf{d}_{12}|^6}\right)\left(\frac{\delta(r_1-R_0)}{R_0^2}\sum_{l_1}\kappa_{l_1}^i\sum_{m_1}S_{m_1}^{l_1}(\boldsymbol{\omega}_1)Y_{l_1m_1}(\hat{\mathbf{r}}_1)\right)\\&\times\left(\frac{\delta(r_2-R_0)}{R_0^2}\sum_{l_2}\kappa_{l_2}^i\sum_{m_2}S_{m_2}^{l_2}(\boldsymbol{\omega}_2)Y_{l_2m_2}(\hat{\mathbf{r}}_2)\right)\\=&\sum_{l_1m_1}\sum_{l_2m_2}S_{m_1}^{l_1}(\boldsymbol{\omega}_1)S_{m_2}^{l_2}(\boldsymbol{\omega}_2)P_{m_1m_2}^{l_1l_2}(\mathbf{d}_{12}),\end{aligned} \tag{22}$$

where

$$P_{m_1m_2}^{l_1l_2}(\mathbf{d})=4\epsilon\kappa_{l_1}^i\kappa_{l_2}^i[\sigma^{12}\hat{P}_{12}(\mathbf{d})-\sigma^6\hat{P}_6(\mathbf{d})], \tag{23}$$

and

$$\hat{P}_n(\mathbf{d})=\int\int d\mathbf{r}_1 d\mathbf{r}_2\frac{\delta(r_1-R_0)}{R_0^2}\frac{\delta(r_2-R_0)}{R_0^2}Y_{l_1m_1}(\hat{\mathbf{r}}_1)Y_{l_2m_2}(\hat{\mathbf{r}}_2)\frac{1}{|\mathbf{r}_1-\mathbf{r}_2+\mathbf{d}|^n}. \tag{24}$$

This expression for $\hat{P}_n(\mathbf{d})$ can be computed using the two-center expansion for $n>1$ (see Appendix B for the details and the definition of the function $a_{l_1l_2l}^n$):

TABLE IV. The fitting values of the experimental quantities (top) and the obtained Lennard-Jones parameters (bottom).

Experimental quantity	The energy difference between the global and the local minima	The energy barrier between the minima in $Pa\bar{3}$ phase	Lattice constant at $T=0$ K	Bulk modulus at $T=0$	Cohesive energy
Fitting value	11 meV	250 meV	14.04 Å	13 GPa	-1.7 eV
LJ parameters	σ	ϵ	κ_6	κ_{10}	κ_{12}
Fitted values	3.695 Å	20.255 K	0.542	32.812	4.969
LLM model	3.407 Å	34.365 K	2.561	19.353	7.887

$$\hat{P}_n(\mathbf{d})=\frac{1}{d^n}\sum_l\ (-1)^{l_2}\left(\frac{(4\pi)^3}{(2l_1+1)(2l_2+1)(2l+1)}\right)^{1/2}C((l_1,0)(l_2,0)(l))C((l_1,m_1)(l_2,m_2)(l))Y_{lm_1+m_2}(-\hat{\mathbf{d}})a^n_{l_1l_2l}\left(\frac{R_0}{d},\frac{R_0}{d}\right). \tag{25}$$

Then

$$P^{l_1l_2}_{m_1m_2}(\mathbf{d})=4\epsilon\kappa^i_{l_1}\kappa^i_{l_2}(-1)^{l_2}\sum_{l=0,6,\ldots}(-1)^l\left(\frac{(4\pi)^3}{(2l_1+1)(2l_2+1)(2l+1)}\right)^{1/2}C[(l_1,0)(l_2,0)(l)]C[(l_1,m_1)(l_2,m_2)(l)]$$
$$\times Y_{lm_1+m_2}(\hat{\mathbf{d}})\left[\left(\frac{\sigma}{d}\right)^{12}a^{12}_{l_1l_2l}\left(\frac{R_0}{d},\frac{R_0}{d}\right)-\left(\frac{\sigma}{d}\right)^{6}a^{6}_{l_1l_2l}\left(\frac{R_0}{d},\frac{R_0}{d}\right)\right]. \tag{26}$$

In this formula the values of σ, ϵ, and κ^i_l for $l=6,10,\ldots$ serve as adjustable parameters (the value of κ^i_0, reflecting the total ''number'' of the interaction centers, is taken to be $60/\sqrt{4\pi}$, as in all earlier models). Below, as before, we consider only the contributions from $l=0,6,10,12$. Thus, our model includes five parameters which we determined by fitting to the experimental values of the lattice constant, bulk modulus, cohesive energy as well as the energy difference and the energy barrier between the global minimum and closest to it local minimum orientational configurations. Since the experimental results for the values of the bulk modulus and the energy barrier differ significantly for different experiments, we have taken as our fitting values the numbers that are somewhere in between the maximum and minimum reported values, e.g., $B=13$ GPa for the bulk modulus and $E_{\rm bar}=250$ meV for the energy barrier. The fitting values as well as obtained parameters σ, ϵ, and κ_l are presented in Table IV. There we have also included for a comparison the values of the corresponding parameters for the LJ part of the LLM model. As one can see, the distribution of the LJ interaction centers over the surface of C_{60} molecule for our model is quite different from the carbon atoms distribution.

The visualization of the resulting distribution of short-range interaction centers is presented in Fig. 4(a)—there the distance from a given point on the depicted surface to the spherical surface of certain radius is equal to the interaction centers density at this point, e.g., the ''hills'' and ''spikes'' correspond to the local maxima of the interaction centers density, while ''pits'' represent its minima. Figure 4(b) represents (in arbitrary units) the density of the interaction centers along the cut through the centers of two pentagonal faces and the center of one of the 6-6 bonds (p, a, d, s, and h correspond to the centers of the pentagons, atomic sites, centers of the 6-6, 6-5, and hexagons, respectively)—it is relatively high for both atomic sites and 6-6 bonds. At the same time, 5-6 bonds correspond to slightly smaller densities, while the centers of pentagonal and hexagonal faces are real ''voids,'' with the centers of the hexagonal faces being slightly ''deeper.'' All this gives us some early insights into possible mutual orientations of two molecules that would minimize their short-range interaction—it should be either atomic site or double bond on one molecule versus the center of the hexagon on the other. As we will show in the next section, those mutual orientations indeed minimize the total interaction energy of two molecules in our model.

The intermolecular potential, constructed as described above, is analyzed in the next section. However, one comment is due here: at this stage we have fitted to 250 meV the value of the potential barrier that the molecule in the $Pa\bar{3}$ phase has to overcome to change its orientation from 22° to 82° by rotating around its local threefold axis, while its nearest neighbors are kept at 22° orientations. In Appendix A we show that this value indeed corresponds to the lowest possible barrier between the two orientations.

IV. PROPERTIES OF THE PROPOSED MODEL

In this section we analyze the various predictions of the proposed model. In particular, we present the predictions about the most favorable mutual orientations of two interacting molecules together with the mean-field stability analysis of the high-temperature phase. In addition, as a test for our model we compute the dispersion curves for the libron excitations in the $Pa\bar{3}$ phase as well as the local orientational

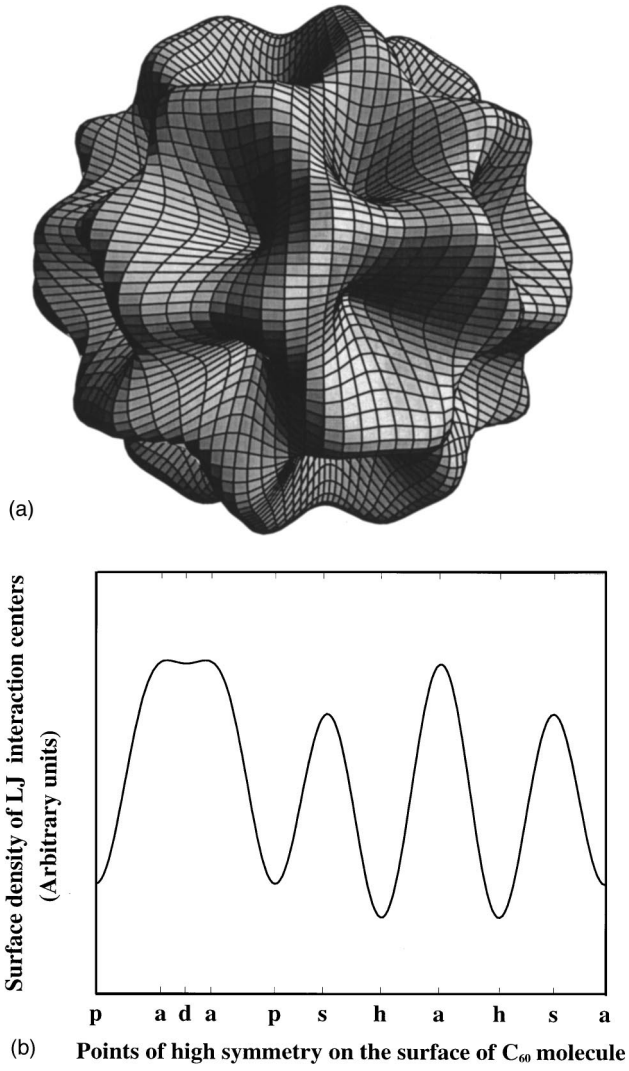

FIG. 4. The distribution of the short-range interaction centers on the surface of C_{60} molecule. The distance from a given point on the depicted surface (a) to the surface of a sphere of certain radius is equal to the interaction centers density at this point. The cut through the centers of the pentagonal faces and the center of the 6-6 bond (b) allows one to see a clear difference between the interaction centers density near atomic sites, 6-6 and 6-5 bonds on the one hand and near the centers of hexagons and pentagons, on the other. The symbols p, a, d, s, and h represent the centers of the pentagons, atomic sites, centers of the 6-6, 6-5, and hexagons, respectively.

order parameters, describing the behavior of molecules in the high-temperature phase. These predictions are compared with the experimental data as well as with similar computations for two of the most frequently used previous models of the interaction potential.

In spite of the existence of quite a few models of the intermolecular interaction, the question of the most favored mutual orientation of two C_{60} molecules has not been investigated in detail. David *et al.*[22] have suggested that the observed symmetry of the low-temperature phase of C_{60} crystals is a reflection of the following property of the intermolecular potential—for two C_{60} molecules the interaction energy is at minimum when the 6-6 bond of one molecule faces the center of the pentagon on the other one. This way, the arrangement of molecules in the low-temperature phase is suggested to optimize all nearest-neighbor interactions without frustration. To verify this assumption, we used our potential to compute the interaction energies for the different mutual orientations of two fullerene molecules. For our analysis we have chosen the orientations, for which the high-symmetry elements of both molecules (center of 6-6 or 6-5 bond or center of hexagonal or pentagonal face or atomic site) lie on the line connecting the molecular centers of gravity. This arrangement, of course, still leaves the choice of the relative angle of rotation, ψ of the molecules around the line connecting their centers. For each of the pairs of symmetry elements we have chosen the angle ψ to minimize the interaction energy. The results (in meV) are summarized in Table V: to make it easier to compare different mutual orientations, we have subtracted from each number there the orientation-independent contribution.

The numbers in Table V lead to an interesting conclusion—the interaction energy for the pair of molecules is minimized when the atomic site of one molecule faces the center of the hexagonal face of the neighboring molecule. This result is not at all surprising—the atomic sites, as well as 6-6 and 6-5 bonds are the places with the maximum of both the Coulomb charge and the LJ interaction centers concentration on the surface of the molecule, while the hexagonal or pentagonal faces play the role of voids. At the same time, in the crystal the ordering motive is quite different: at room temperature the molecules rotate so fast that the influence of the orientation-dependent part of the intermolecular potential on the translational ordering of molecules can be safely ignored and therefore, the crystal follows the closed-

TABLE V. The computed pair interaction energy (in meV) for various mutual orientations of two C_{60} molecules.

Elements	6-6	6-5	Hexagon	Pentagon	Atom
6-6	38	12	−35	−22	31
6-5	12	−6	−28	-19	12
Hexagon	−35	−28	−5	−10	−36
Pentagon	−22	−19	−10	−12	−23
Atom	31	12	−36	−23	10

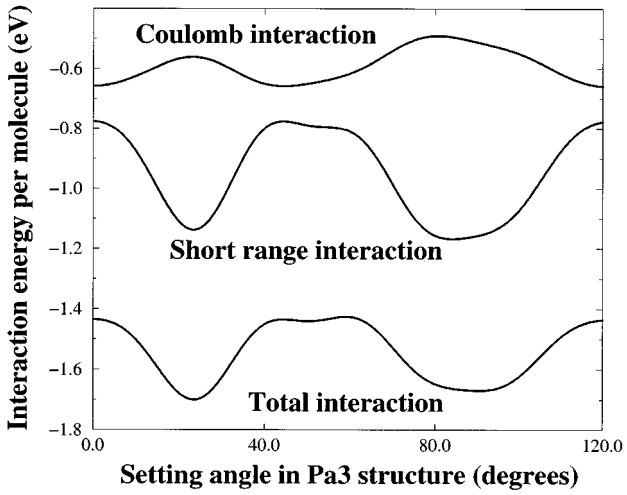

FIG. 5. The Coulomb, short-range and the total potential energy per molecule as a function of the setting angle in the $Pa\bar{3}$ phase, according to our model. The global minimum in energy corresponds to the setting angle of 23.5°.

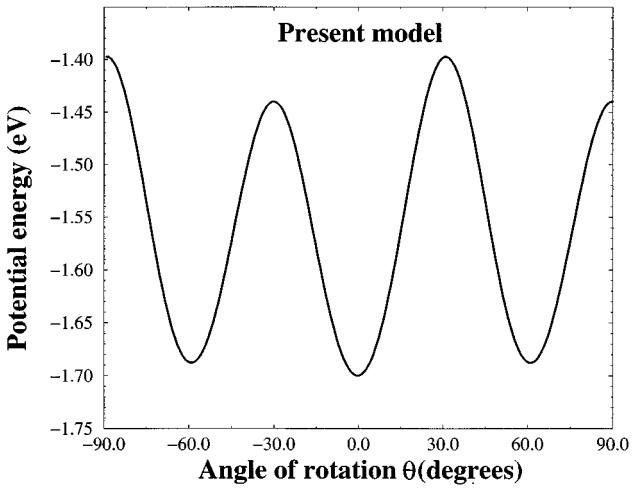

FIG. 6. The potential energy of a molecule in the $Pa\bar{3}$ phase as the function of the rotation angle θ around local threefold axis, according to our model. The nearest-neighbor molecules are kept in their ''global minimum'' orientations with the setting angles of 23.5°. Here $\theta=0$ corresponds to the global minimum orientation of the rotated molecule.

packing scenario to adopt an fcc structure. As the temperature is lowered, the orientation-dependent part of the interaction becomes more and more important. However, the molecules find themselves in an awkward situation, when minimizing pair interaction energy with some of the nearest neighbors is penalized through pair interactions with the rest of the neighbors. In view of this frustration the crystal adopts the $Pa\bar{3}$ spatial structure. In Fig. 5 we have plotted the variation of the computed Coulomb, short-range, and total intermolecular interaction energy in the $Pa\bar{3}$ phase as a function of the setting angle. We find that the total intermolecular interaction potential, obtained by combining the microscopic Coulomb and the proposed empirical short-range interactions, has a global minimum at the setting angle of 23.5°, in agreement with the experimental findings. Figure 6 shows what our model predicts for the potential energy of the molecule in the $Pa\bar{3}$ structure as the function of the rotation angle θ around its local threefold axis, when the neighboring molecules are kept in their ''global minimum'' orientations with the setting angles of 23.5°. The local minimum, closest in energy to the global one, corresponds to $\theta\approx 60°$.

As we will show, the $Pa\bar{3}$ spatial structure is indeed the best compromise between the ''preset'' fcc translational order and the orientational part of the pair intermolecular potential. To investigate this point, we have performed the stability analysis of the high-temperature phase using the mean-field approach. The detailed description of the procedure is outlined by Heid,[45] therefore in this paper we will limit ourselves to a brief restatement of the major theoretical steps along with the results of the computations using our model.

First of all, in order to simplify the group-theoretical analysis of the instabilities in the potential, one re-expresses the interaction between the molecules in terms of molecular rotator functions,[35] representing both the molecular symmetry and the symmetry of cubic lattice:

$$U_{l\mu}(\boldsymbol{\omega})=\sum_{m_1} S^{l}_{m_1}(\boldsymbol{\omega})c^{*l}_{\mu m_1}=\sum_{m_1 m_2} a_{lm_2}D^{l}_{m_1 m_2}(\boldsymbol{\omega})c^{*l}_{\mu m_1}, \tag{27}$$

where μ labels the basis functions for the irreducible representations of the O_h group and $\boldsymbol{\omega}$ is a vector of three Euler angles. The coefficients $c^{l}_{\mu m_1}$ are tabulated by Bradley and Cracknell.[46] The functions $U_{l\mu}(\boldsymbol{\omega})$ form an orthogonal set:

$$\int U_{l_1\mu_1}(\boldsymbol{\omega})U_{l_2\mu_2}(\boldsymbol{\omega})d\boldsymbol{\omega}=\frac{8\pi^2}{2l_1+1}\delta_{l_1 l_2}\delta_{\mu_1\mu_2}. \tag{28}$$

Then the interaction between molecules i and j can be written as

$$\begin{aligned} V(\mathbf{d}_i,\boldsymbol{\omega}_i,\mathbf{d}_j,\boldsymbol{\omega}_j)&=\sum_{l_1 m_1}\sum_{l_2 m_2} S^{l_1}_{m_1}(\boldsymbol{\omega}_i)S^{l_2}_{m_2}(\boldsymbol{\omega}_j)Q^{l_1 l_2}_{m_1 m_2}(\mathbf{d}_{ij}) \\ &=\sum_{l_1\mu_1}\sum_{l_2\mu_2} U_{l_1\mu_1}(\boldsymbol{\omega}_i)U_{l_2\mu_2}(\boldsymbol{\omega}_j)W^{l_1 l_2}_{\mu_1\mu_2}(\mathbf{d}_{ij}), \end{aligned} \tag{29}$$

with

$$W^{l_1 l_2}_{\mu_1\mu_2}(\mathbf{d}_{ij})=\sum_{m_1 m_2} c^{l_1}_{\mu_1 m_1}c^{l_2}_{\mu_2 m_2}Q^{l_1 l_2}_{m_1 m_2}(\mathbf{d}_{ij}). \tag{30}$$

Within the mean-field approach the orientational potential energy of the molecule on site i is given by the expression:

$$\begin{aligned} V^{i}_{\mathrm{MF}}(\boldsymbol{\omega})&=\sum_{j,l_1,\mu_1,l_2,\mu_2}{}' W^{l_1 l_2}_{\mu_1\mu_2}(\mathbf{d}_{ij})\langle U^{j}_{l_2\mu_2}\rangle U_{l_1\mu_1}(\boldsymbol{\omega}) \\ &\equiv\sum_{l_1\mu_1}{}' v_{l_1\mu_1}U_{l_1\mu_1}(\boldsymbol{\omega})+\sum_{j,l_1,\mu_1,l_2,\mu_2}{}'' W^{l_1 l_2}_{\mu_1\mu_2}(\mathbf{d}_{ij}) \\ &\quad\times\langle U^{j}_{l_2\mu_2}\rangle U_{l_1\mu_1}(\boldsymbol{\omega}), \end{aligned} \tag{31}$$

where the averages $\langle U^{i}_{l\mu}\rangle$ are taken with respect to the MF orientational distribution function $f^{i}_{\mathrm{MF}}(\boldsymbol{\omega})=\exp(-\beta V^{i}_{\mathrm{MF}}(\boldsymbol{\omega}))$. The primes on the summations exclude

TABLE VI. The calculated values of the orientational order parameters for our model compared to the other interaction models.

Values of γ_l	γ_6	γ_{10}	γ_{12}^1	γ_{12}^2
Experimental values	−0.386	0.217	0.159	0.440
Values from our model	−0.072	0.218	0.044	0.190
Values from LLM model	0.421	0.132	0.081	0.368
Lamoen and Michel (Ref. 9)	−0.130	0.636	0.049	0.242
Lamoen and Michel (Ref. 10)	−0.430	0.840	0.038	0.599

$l_1=l_2=0$ in the first line and $l_1=0$ in the second line, while the double primed summation is carried out over nonzero values of both indices l_1 and l_2. Here the contribution from the crystal field is shown explicitly, and the index $\mu=(\rho 1)$ stands for the ρth A_{1g} irreducible representation of the O_h group (for $l=6,10$ there is only $\rho=1$, while for $l=12$ there are two irreducible representations with A_{1g} symmetry, labeled as $\rho=1$ and $\rho=2$).

For a given temperature this set of equations has many solutions with different symmetry properties. The solution that minimizes the free energy at high temperatures has full cubic symmetry, that is $\langle U_{l\mu}^j\rangle=(\gamma_l^\rho/\kappa_l)\,\delta_{\mu,(\rho 1)}$, where κ_l are defined in Eq. (9). The mean-field orientational potential for any molecule in the crystal becomes

$$V_{\mathrm{MF}}(\boldsymbol{\omega})=\sum_{l\rho} v_{l\rho}^{\mathrm{MF}} U_{l(\rho 1)}(\boldsymbol{\omega}), \tag{32}$$

where

$$v_{l\rho}^{\mathrm{MF}}=v_{l\rho}+\sum_j {\sum_{l_1\rho_1}}'' W_{(\rho 1)(\rho_1 1)}^{ll_1}(\mathbf{d}_{ij})\frac{\gamma_{l_1}^{\rho_1}}{\kappa_l}. \tag{33}$$

This equation together with

$$\frac{\gamma_{l_1}^{\rho_1}}{\kappa_l}=\frac{\int d\boldsymbol{\omega} U_{l_1(\rho_1 1)}(\boldsymbol{\omega})\exp[-\beta(\Sigma_{l\rho} v_{l\rho}^{\mathrm{MF}} U_{l(\rho 1)}(\boldsymbol{\omega}))]}{\int d\boldsymbol{\omega}\exp[-\beta(\Sigma_{l\rho} v_{l\rho}^{MF} U_{l(\rho 1)}(\boldsymbol{\omega}))]} \tag{34}$$

form the set of nonlinear equations for $\gamma_{l_1}^{\rho_1}$ as a function of $\beta=1/(k_BT)$. For $T=300$ K one can simplify the problem by expanding the exponent. For our potential this results in a rapidly converging series. That is, keeping terms, containing β^2 changes the solutions for $\gamma_{l_1}^{\rho_1}$ only by few percent compared to the ones resulting from keeping terms linear in β. For our calculations we have used the value $a=14.16$ Å, as the fcc lattice constant for room temperature.[36] Our results are summarized in Table VI. In order to compare our predictions with those from other models, we have also included in this table the values of the orientational order parameters for the same temperature and lattice constant, predicted by the LLM model[5] and the models of Michel and co-workers.[9–11] For the former model we have computed the crystal-field values $v_{l\rho}$ and have used the high-temperature expansion[9] to get the values of γ_l^ρ. The latter model included 210 centers on the atomic sites as well as 6-5 and 6-6 bonds of each molecule, interacting via Lennard-Jones 12-6 potential. In the later papers[10,11] to improve the agreement with the experiment, the 12 part was replaced by the Born-Mayer repulsive potential and the 6 part was limited to include the attraction only between the atomic site centers. In both papers at least nine Born-Mayer and/or Lennard-Jones parameters were chosen in such a way that the predicted values of the crystal field coefficients would be as close to the experimental ones as possible—compared to five adjustable parameters of our model. We have again employed the high-temperature expansion to convert the crystal-field coefficients $w_l^{\tau_{1g}}$ (analogous to our $v_{l\rho}$) of Ref. 9 into γ_l^ρ.

Comparing with the experimental data from Table I, one can see that our model gives the proper signs of all of the measured orientational order parameters and that numerical values are in a reasonable agreement with the experiments. While the latest version of the model proposed by Michel *et al.*[11] has a better value of γ_6, their value for γ_{10} is too high. At the same time, the orientational order-parameter values from the model of Lu *et al.* are in the qualitative disagreement with the experiment: the sign of γ_6 is of crucial importance for the shape of the mean-field orientational potential.[10,11]

The most likely low-temperature structures within the mean-field approach can be identified by looking at the eigenvalue spectrum of the orientational susceptibility matrix, obtained by keeping the quadratic terms with respect to the orientational order parameters in the Landau expansion of the free energy. Here we adopt an equivalent approach,[45] based on the analysis of the eigenvalue spectrum of

$$W_{\mu_1\mu_2}^{l_1l_2}(\mathbf{q})=\frac{1}{N}\sum_{\mathbf{d}_i,\mathbf{d}_j}\sum_{l_3\mu_3} W_{\mu_1\mu_3}^{l_1l_3}(\mathbf{d}_{ij}) J_{\mu_3\mu_2}^{l_3l_2}\exp(i\mathbf{q}(\mathbf{d}_j-\mathbf{d}_i)), \tag{35}$$

where

$$J_{\mu_1\mu_2}^{l_1l_2}=\langle U_{l_1\mu_1}^j U_{l_2\mu_2}^j\rangle-\langle U_{l_1\mu_1}^j\rangle\langle U_{l_2\mu_2}^j\rangle. \tag{36}$$

The averages in the last expression are taken with respect to the high-temperature distribution function $f_{\mathrm{MF}}(\boldsymbol{\omega})$. The values of $\langle U_{l\mu}^j\rangle$ in this phase do not depend on position of the site j and are equal to γ_l^ρ/κ_l. At the same time, the averages $\langle U_{l_1\mu_1}^j U_{l_2\mu_2}^j\rangle$ can be expressed in terms of $\langle U_{l\mu}^j\rangle$ in the following way (see Appendix C):

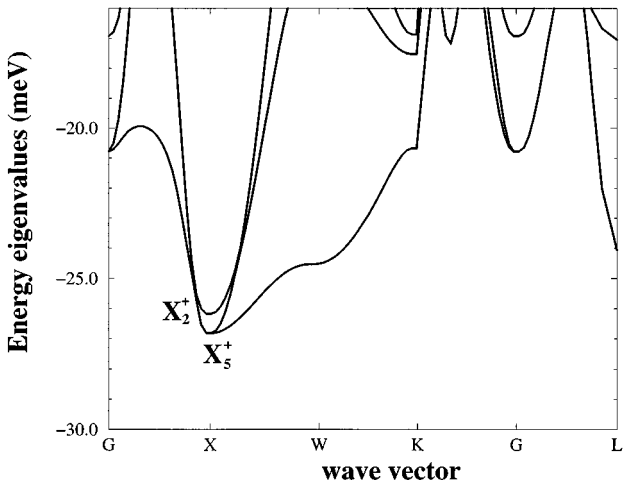

FIG. 7. The lowest eigenvalues of the interaction matrix for wave vectors along the lines of high symmetry in the first Brillouin zone of the fcc lattice.

$$\langle U^j_{l_1\mu_1} U^j_{l_2\mu_2}\rangle = \frac{\delta_{l_1 l_2}\delta_{\mu_1\mu_2}}{2l_1+1} + \sum_{l\rho} \langle U^j_{l(\rho 1)}\rangle M_{l_1 l_2 l} N^{\mu_1\mu_2(\rho 1)}_{l_1 l_2 l}, \tag{37}$$

where

$$M_{l_1 l_2 l} = \sum_{n_1 n_2} a_{l_1 n_1} a_{l_2 n_2} a_{l, n_1+n_2} C((l_1 n_1)(l_2 n_2)(l)), \tag{38}$$

and

$$N^{\mu_1\mu_2(\rho 1)}_{l_1 l_2 l} = \sum_{n_1 n_2} c^{l_1 *}_{\mu_1 n_1} c^{l_2 *}_{\mu_2 n_2} c^{l}_{(\rho 1), n_1+n_2} C((l_1 n_1)(l_2 n_2)(l)). \tag{39}$$

The lowest-energy part of the resulting eigenvalue spectrum of $W^{l_1 l_2}_{\mu_1\mu_2}(\mathbf{q})$ is shown in Fig. 7. As we see, our model predicts that the strongest instability in the intermolecular potential occurs at the $\underline{X}$ point of the reciprocal lattice and corresponds to the $Pa3$ space group. This result remained unchanged when we varied the value of the lattice constant, used in the calculation—however, the actual energy eigenvalues strongly depend on this parameter—for example, for a slightly different lattice constant $a = 14.18$ Å, we obtained $E(X_5^+) = 21.6$ meV. The closest competing instability (also occurring at the X point) corresponds to the tetragonal $P4_2/mnm$ space group. This instability may be responsible for the recently observed noncubic peaks in the diffuse x-ray and quasielastic neutron-scattering patterns of C_{60} single crystals in the high-temperature phase.[47–49]

A corresponding analysis for the potentials similar to the LLM model was performed by Heid.[45] He showed that the sequence of phase transitions associated with these potentials does not correspond to the one observed in experiments. In particular, unobserved intermediate phases are predicted. At the same time, to the best of our knowledge, there were no reports on the stability analysis of the models proposed by Michel and Lamoen, and this prevents us from making a direct comparison with their model.

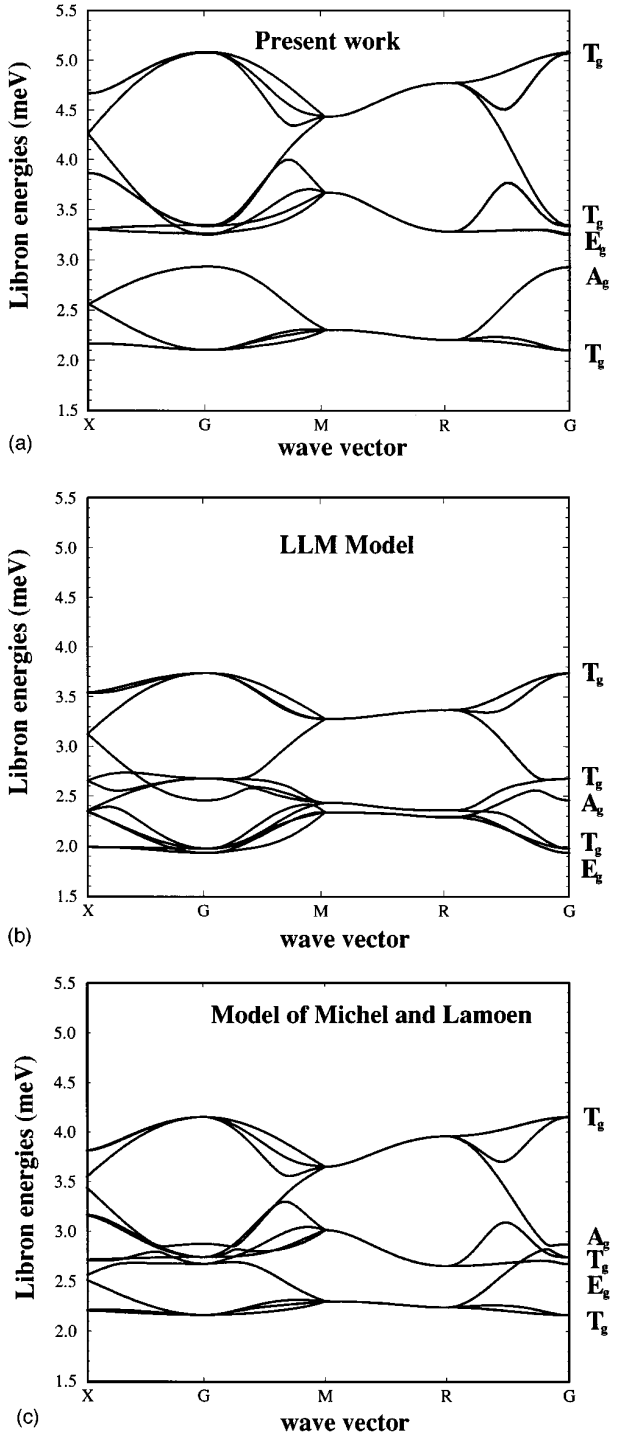

FIG. 8. The libron dispersion relations for wave vectors along the lines of high symmetry in the first Brillouin zone of the simple cubic lattice for the present model (a), LLM (b) and the model of Lamoen and Michel (c). The details of the mode symmetry assignment are given in the paper by Yildirim and Harris (Ref. 50). The curves for the LLM potential have been corrected by a factor of $\sqrt{2}$ (Ref. 39) compared to the ones presented in Refs. 50 and 51.

Another important test for the interaction potential is to compare the computed frequencies of the libron excitations with the experimental ones. Figure 8 presents the libron dispersion curves for our model as well as the models of LLM and Michel and Lamoen along the high-symmetry lines in

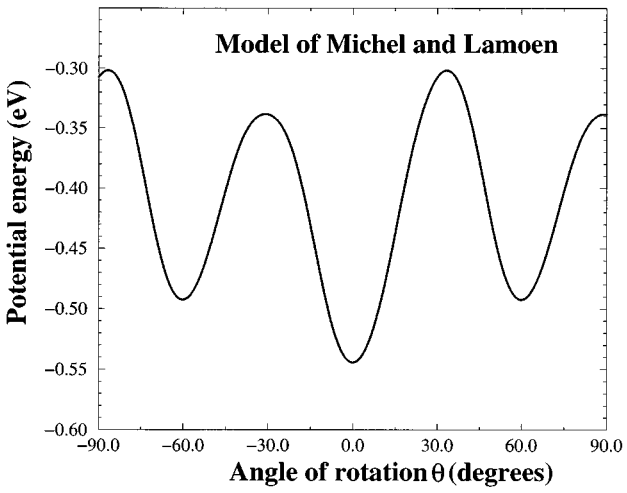

FIG. 9. The potential energy of the molecule in the $Pa\bar{3}$ phase as the function of the rotation angle θ around local threefold axis, according to the model of Lamoen and Michel. Compare with Fig. 6.

the first Brillouin zone. The extensive symmetry analysis of the libron modes in C_{60} crystals was performed by Yildirim and Harris.[50] In the present paper we are following the same notation for the symmetry points in the reciprocal lattice and for the symmetry labels of the modes (E_g, T_g, A_g). Also, we have added the factor $\sqrt{2}$ that was missing[39] in the libron energies, reported in Refs. 50 and 51. Comparing the computed dispersion curves with the experimental results,[37–41] one can see that our model reproduces some, but not all, of the observed features of the spectrum. In particular, the computed frequency of the A_g mode at the G point is in very good agreement with the experimental value [$\omega_{\mathrm{exp}} = 3.04$ meV (Ref. 39)]. Note that the A_g mode corresponds to varying the setting angle in the $Pa\bar{3}$ phase. The fact that our theory correctly reproduces the frequency of this mode suggests that the barrier of rotation around the [1,1,1] axis is correctly represented by our potential. However, our calculation predicts that the lowest-frequency librons at the G point have T_g symmetry, whereas the experimental interpretation attributes E_g symmetry to these modes. We have investigated a range of parameters for our model but are unable to remove this disagreement. Furthermore, the model of Lamoen and Michel,[10,11] which captures some features of the potential correctly, gives the same prediction as ours for the symmetry of the lowest-energy modes. Of course, one has to keep in mind that our calculation of the libron modes does not allowfor any orientational disorder, which is observed in C_{60} crystals even at very low temperatures. An additional investigation is necessary in order to determine whether the presence of orientational disorder can account for the discrepancy between theory and experiment mentioned above.

Before concluding, we would like to point out that the phenomenological model of Lamoen and Michel, constructed to obtain reasonable values of the orientational order parameters in the high-temperature phase, does not give correct predictions as far as the low-temperature phase is concerned. As an illustration, in Fig. 9 we show the potential

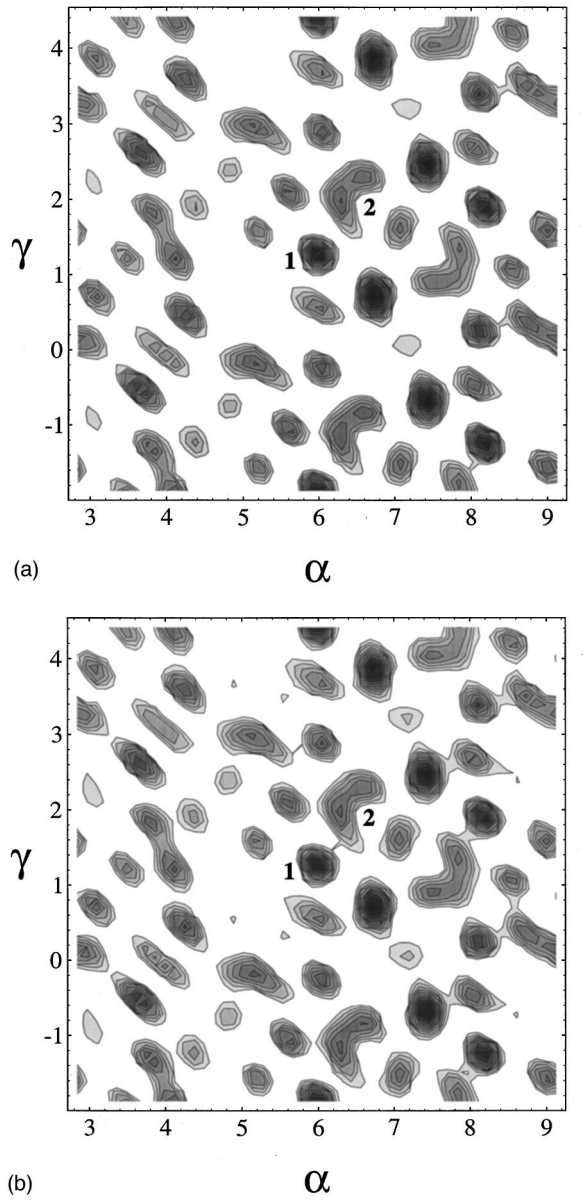

FIG. 10. The contour plots of the potential energy of C_{60} molecule in the $Pa\bar{3}$ phase (all neighbors are kept in their ''global minimum'' orientations) for a fixed Euler angle $\beta = 1.15$ rad as a function of α and γ. The regions, shown on the graphs correspond to the values of the potential energy from -1.7 eV (global minimum) to -1.689 eV (local minimum) plus the ''barrier'' of (a) 240 meV and (b) 250 meV.

energy of a molecule in the $Pa\bar{3}$ phase computed for this model when the molecule is rotated around its local threefold axes. The lattice constant for this calculation was taken to be equal to the experimental value of 14.04 Å rather than the unrealistic value of 14.68 Å predicted by this model. We would like to point out that, while this value could be corrected by adding the appropriate orientationally independent contribution to the potential, such a modification will not change the deficiencies in the orientational behavior of this model, namely that both the relative energies of two minima as well as the value of the barrier between them is in signifi-

cant disagreement with the experimental values shown in Table I.

V. CONCLUSION

We have constructed a model of the interaction potential for C_{60} molecules which agrees with the quantum-chemical calculations of the C_{60} molecular charge densities and the details of the crystal structure at low temperatures. We may summarize our work as follows.

(1) The earlier models of the interaction potential do not properly describe the Coulomb interaction between the C_{60} molecules. The major reason for this lies in the *ad hoc* character of the ''bond charges,'' inconsistent with the microscopic molecular charge distribution. In addition, we have determined that the Coulomb interaction between the neighboring C_{60} molecules at the separations typical for solids does not reduce to the multipole-multipole coupling and that the proper treatment of the charge overlaps between the molecules is necessary.

(2) The short-range part of the interaction is best modeled by the 12-6 Lennard-Jones interactions between the interaction centers distributed over the surfaces of the molecules. The proper choice of the fitting parameters have yielded the potential with the best overall behavior with respect to the experimental results for both high- and low-temperature phases.

(3) The proposed interaction potential favors the ''atomic site versus hexagon'' mutual orientation of the two interacting molecules, contrary to the argument in Ref. 22. In the crystal, however, it is impossible to optimize the interactions between all the nearest-neighbor pairs in this way. In the resulting frustration, the $Pa\bar{3}$ space structure was found to be the best candidate for the low-temperature phase.

(4) The present model shows that stabilization of the $Pa\bar{3}$ phase at low temperatures is accompanied by a close competition with other phases. This prediction may be related to the recently observed noncubic peaks in the diffuse x-ray and neutron-scattering patterns taken at temperatures close to the orientational ordering transition.[47–49]

(5) We report the microscopic values of the molecular multipole density functions $\rho_l(r)$ to make them available for the future research. The results obtained in this work can be used in the theoretical studies of orientational ordering of C_{60} monolayers[52] as well as orientational ordering in the crystals comprised of C_{60} derivatives.[53,54]

ACKNOWLEDGMENTS

We acknowledge useful conversations with J. E. Fischer, P. A. Heiney, E. J. Mele, P. Launois, and S. Ravy. Partial support for this work was provided by the National Science Foundation under Grant No. NSF-95-20175.

APPENDIX A: THE MINIMUM ENERGY BARRIER BETWEEN THE GLOBAL AND THE LOCAL MINIMA IN LOW-TEMPERATURE PHASE

In order to find the lowest possible energy barrier that the molecule has to overcome to get to the $Pa\bar{3}$ global minimum arrangement, where all molecules are kept at the setting angle of $\approx 22°$, from the local minimum, where the setting angle of one molecule is changed to $\approx 82°$, we have computed the orientational potential energy $V(\alpha,\beta,\gamma)$ of the molecule, when its nearest neighbors are kept at the global minimum setting angles. To visualize our results, below we present the contour plots of the potential energy—the three-dimensional space of the Euler angles was ''sliced'' along the planes of constant β, so that each plot represents the dependence of the potential energy on α and γ with β being fixed. The way we plot our data is such that the points in the space of Euler angles, whose energies are higher than certain value, are not shown. The regions in the space of Euler angles enclosing the global and local minima plus all neighboring points, whose energies are not higher than the limiting value mentioned above, form wormlike ''islands.'' As the limiting value is pushed up, the islands grow, and when the critical limiting value is reached, there occurs a percolation between the local minimum island and the global minimum one. Thus, this critical limiting value is equal to the energy of the molecule at the local minimum plus an orientational barrier between the local and the global minima. Each β ''slice'' represents the cross sections of islands and for a given limiting value one has to scan through all slices, cutting the local minimum island, in order to check that it is disconnected from any other island. When the limiting value becomes equal to the orientational barrier, the percolation happens first on one of the β slices. In Fig. 10 we show the contour plots of the potential energy for this value of $\beta = 1.15$ rad for two limiting values: (a) -1.689 eV$+240$ meV, (b) -1.689 eV$+250$ meV. Our ''best slice'' contains both the local and the global minima regions—marked on the plots as 1 and 2, respectively. As one can see, when the ''trial barrier'' is set to 240 meV, the islands remain completely isolated, whereas when we switch to 250 meV, there occurs a percolation between neighboring islands.

APPENDIX B: TWO-CENTER EXPANSION AND COMPUTATION OF THE INTERACTION MATRICES

Yasuda and Yamamoto[55] have shown, that for $|\mathbf{r}_1|+|\mathbf{r}_2|<\mathbf{d}$ the function containing the inverse powers of $|\mathbf{r}_1-\mathbf{r}_2+\mathbf{d}|$ can be represented by the expansion (for $n>1$)

$$\frac{1}{|\mathbf{r}_1-\mathbf{r}_2+\mathbf{d}|^n}=\frac{1}{d^n}\sum_{l_3}\sum_{l_4}\sum_{l}(-1)^{l_4}\left(\frac{(4\pi)^3}{(2l_3+1)(2l_4+1)(2l+1)}\right)^{1/2}C((l_3,0)(l_4,0)(l))a^n_{l_3l_4l}\left(\frac{r_1}{d},\frac{r_2}{d}\right)$$

$$\times\sum_{m_3m_4}C((l_3,m_3)(l_4,m_4)(l))Y_{l,m_3+m_4}(-\hat{\mathbf{d}})Y^*_{l_3m_3}(\hat{\mathbf{r}}_1)Y^*_{l_4m_4}(\hat{\mathbf{r}}_2), \tag{B1}$$

where $C((l_3,m_3)(l_4,m_4)(l))$ are Clebsch-Gordan coefficients and

$$a^{n}_{l_3 l_4 l}(x,y)=\sum_{p}\ \sum_{q}\ \frac{x^p y^q (2l_3+1)(2l_4+1)}{(n-2)!(p-l_3)!!}\ \frac{(n+p+q-l-3)!!}{(p+l_3+1)!!(q-l_4)!!}\ \frac{(n+p+q+l-2)!!}{(q+l_4+1)!!} \tag{B2}$$

with the sum for p going over $l_3, l_3+2, l_3+4 \ldots$, etc., and for q— over $l_4, l_4+2, l_4+4, \ldots$, etc.

For $n=1$ the above equation becomes

$$\begin{aligned}\frac{1}{|\mathbf{r}_1-\mathbf{r}_2+\mathbf{d}|}=\frac{1}{d}\sum_{l_3}\ \sum_{l_4}\ (-1)^{l_4}\left(\frac{(4\pi)^3}{(2l_3+1)(2l_4+1)(2(l_3+l_4)+1)}\right)^{1/2}\left(\frac{r_1}{d}\right)^{l_3}\left(\frac{r_2}{d}\right)^{l_4} C((l_3,0)(l_4,0)(l_3+l_4))\\ \times\frac{(2l_3+1)(2l_4+1)(2(l_3+l_4)-1)!!}{(2l_3+1)!!(2l_4+1)!!}\sum_{m_3 m_4} C((l_3,m_3)(l_4,m_4)(l_3+l_4))Y_{l_3+l_4,m_3+m_4}(-\hat{\mathbf{d}})\\ \times Y^{*}_{l_3 m_3}(\hat{\mathbf{r}}_1)Y^{*}_{l_4 m_4}(\hat{\mathbf{r}}_2).\end{aligned} \tag{B3}$$

Using this result we can compute the Coulomb interaction matrix $R^{l_1 l_2}_{m_1 m_2}(\mathbf{d})$ for the core and the total charges on the neighboring molecules:

$$\begin{aligned}R^{l_1 l_2}_{m_1 m_2}(\mathbf{d})=(-1)^{l_1}4\frac{|e|}{d}\left(\frac{R_0}{d}\right)^{l_2}\kappa_{l_2}\left[\int\left(\frac{r_1}{d}\right)^{l_1}[\rho^{\mathrm{core}}_{l_1}(r_1)+\rho^{\mathrm{val}}_{l_1}(r_1)]r_1^2 dr_1\right]\left(\frac{(4\pi)^3}{(2l_1+1)(2l_2+1)[2(l_1+l_2)+1]}\right)^{1/2}\\ \times C((l_1,0)(l_2,0)(l_1+l_2))\frac{(2l_1+1)(2l_2+1)[2(l_1+l_2)-1]!!}{(2l_1+1)!!(2l_2+1)!!}C((l_1,m_1)(l_2,m_2)(l_1+l_2))Y_{l_1+l_2,m_1+m_2}(\hat{\mathbf{d}}).\end{aligned} \tag{B4}$$

The integral in the last expression is directly related to the ''reduced'' multipole moments q_{lm},[8] namely

$$\int r^2 dr\left(\frac{r}{d}\right)^{l}[\rho^{\mathrm{core}}_{l}(r)+\rho^{\mathrm{val}}_{l}(r)]=\left(\frac{R_0}{d}\right)^{l}\frac{q_{lm}|e|}{a_{lm}}. \tag{B5}$$

Further, since the ratio q_{lm}/a_{lm} does not depend on m, we can choose, say, $m=0$. Then we obtain Eq. (10).

In the same way one can compute the values of $\hat{P}_n(\mathbf{d})$ for the expression of the Lennard-Jones interaction matrix $P^{l_1 l_2}_{m_1 m_2}(\mathbf{d})$ from Eq. (25).

APPENDIX C: COMPUTATIONS OF ORIENTATIONAL CORRELATIONS

The computation of the averages $\langle U^{j}_{l_1\mu_1}U^{j}_{l_2\mu_2}\rangle$ in the high-temperature phase can be simplified in the following way. The mean-field orientational distribution function $f_{\mathrm{MF}}(\boldsymbol{\omega})$ above the orientational ordering transition has full cubic symmetry:

$$f_{\mathrm{MF}}(\boldsymbol{\omega})=\exp(-\beta V_{\mathrm{MF}}(\boldsymbol{\omega}))=\exp\left(-\beta\sum_{l\rho}\ v^{\mathrm{MF}}_{l\rho}U_{l(\rho 1)}(\boldsymbol{\omega})\right)\equiv\sum_{l\rho}\ Z^{\mathrm{MF}}_{l\rho}(\beta)U_{l(\rho 1)}(\boldsymbol{\omega}). \tag{C1}$$

Since functions $U_{l(\rho 1)}(\boldsymbol{\omega})$ form an orthogonal set, the orientational partition function is given by

$$Q_{\mathrm{MF}}(\beta)=\int d\boldsymbol{\omega} f_{\mathrm{MF}}(\boldsymbol{\omega})=8\pi^2 Z^{\mathrm{MF}}_{0}(\beta) \tag{C2}$$

and the averages $\langle U_{l(\rho 1)}\rangle$ are equal to

$$\langle U_{l(\rho 1)}\rangle=\frac{1}{Q_{\mathrm{MF}}}\int d\boldsymbol{\omega}U_{l\rho 1}(\boldsymbol{\omega})f_{\mathrm{MF}}(\boldsymbol{\omega})=\frac{1}{2l+1}\frac{Z^{\mathrm{MF}}_{l\rho 1}(\beta)}{Z^{\mathrm{MF}}_{0}(\beta)}. \tag{C3}$$

Similarly,

$$\begin{aligned}\langle U_{l_1\mu_1}U_{l_2\mu_2}\rangle=\frac{1}{Q_{\mathrm{MF}}}\int d\boldsymbol{\omega}U_{l_1\mu_1}(\boldsymbol{\omega})U_{l_2\mu_2}(\boldsymbol{\omega})f_{\mathrm{MF}}(\boldsymbol{\omega})=\sum_{l\rho 1}\ \frac{2l+1}{8\pi^2}\langle U_{l(\rho 1)}\rangle\int d\boldsymbol{\omega}U_{l_1\mu_1}(\boldsymbol{\omega})U_{l_2\mu_2}(\boldsymbol{\omega})U_{l(\rho 1)}(\boldsymbol{\omega})\\ =\frac{\delta_{l_1 l_2}\delta_{\mu_1\mu_2}}{2l_1+1}+\frac{1}{8\pi^2}{\sum_{l\rho}}'(2l+1)\langle U_{l(\rho 1)}\rangle F^{l\rho}_{l_1\mu_1,l_2\mu_2},\end{aligned} \tag{C4}$$

with

$$F^{l\rho}_{l_1\mu_1,l_2\mu_2} = \int d\boldsymbol{\omega} U_{l_1\mu_1}(\boldsymbol{\omega}) U_{l_2\mu_2}(\boldsymbol{\omega}) U_{l(\rho 1)}(\boldsymbol{\omega})$$

$$= \sum_{n_1 m_1} \sum_{n_2 m_2} \sum_{nm} a_{l_1 n_1} a_{l_2 n_2} a_{ln} c^{l_1 *}_{\mu_1 m_1} c^{l_2 *}_{\mu_2 m_2} c^{l}_{(\rho 1)m} \int d\omega D^{l_1}_{m_1 n_1}(\omega) D^{l_2}_{m_2 n_2}(\omega) D^{l *}_{mn}(\omega)$$

$$= \frac{8\pi^2}{2l+1} \sum_{n_1 m_1} \sum_{n_2 m_2} \sum_{nm} a_{l_1 n_1} a_{l_2 n_2} a_{ln} c^{l_1 *}_{\mu_1 m_1} c^{l_2 *}_{\mu_2 m_2} c^{l}_{(\rho 1)m} C((l_1,m_1)(l_2,m_2)(l)) C((l_1,n_1)(l_2,n_2)(l))$$

$$= \frac{8\pi^2}{2l+1} M_{l_1 l_2 l} N^{\mu_1 \mu_2 (\rho 1)}_{l_1 l_2 l}, \tag{C5}$$

where

$$M_{l_1 l_2 l} = \sum_{n_1 n_2} a_{l_1 n_1} a_{l_2 n_2} a_{l, n_1+n_2} C((l_1 n_1)(l_2 n_2)(l)), \tag{C6}$$

and

$$N^{\mu_1 \mu_2 (\rho 1)}_{l_1 l_2 l} = \sum_{n_1 n_2} c^{l_1 *}_{\mu_1 n_1} c^{l_2 *}_{\mu_2 n_2} c^{l}_{(\rho 1), n_1+n_2} C((l_1 n_1)(l_2 n_2)(l)). \tag{C7}$$

[1] P. A. Heiney, J. E. Fischer, A. R. McGhie, W. J. Romanow, A. M. Denenstein, J. P. McCauley, Jr., A. B. Smith III, and D. E. Cox, Phys. Rev. Lett. **66**, 2911 (1991).

[2] A. Cheng and M. L. Klein, J. Phys. Chem. **95**, 6750 (1991).

[3] Y. Guo, N. Karasawa, and W. A. Goddard III, Nature (London) **351**, 464 (1991).

[4] A. Cheng and M. L. Klein, Phys. Rev. B **45**, 1889 (1992).

[5] J. P. Lu, X.-P. Li, and R. M. Martin, Phys. Rev. Lett. **68**, 1551 (1992).

[6] M. Sprik, A. Cheng, and M. L. Klein, J. Phys. Chem. **96**, 2027 (1992).

[7] J. D. Axe, S. C. Moss, and D. A. Neumann, in *Solid State Physics: Advances in Research and Applications*, edited by H. Ehrenreich and F. Spaepen (Academic, New York, 1994), Vol. 48, p. 216.

[8] T. Yildirim, A. B. Harris, S. C. Erwin, and M. R. Pederson, Phys. Rev. B **48**, 1888 (1993).

[9] D. Lamoen and K. H. Michel, Z. Phys. B **92**, 323 (1993).

[10] D. Lamoen and K. H. Michel, J. Chem. Phys. **101**, 1435 (1994).

[11] K. H. Michel, D. Lamoen, and W. I. F. David, Acta Crystallogr. A **51**, 365 (1995).

[12] B. P. Feuston, W. Andreoni, M. Parrinello, and E. Clementi, Phys. Rev. B **44**, 4056 (1991).

[13] N. Troullier and J. L. Martins, Phys. Rev. B **46**, 1754 (1992).

[14] D. P. DiVincenzo, E. J. Mele, and N. A. W. Holzwarth, Phys. Rev. B **27**, 2458 (1982).

[15] G. C. La Rocca, Europhys. Lett. **25**, 5 (1994).

[16] T. Yildirim, in *International Winterschool on Electronic Properties of Novel Materials*, edited by H. Kuzmany, J. Fink, M. Mehring, and S. Roth (World Scientific, Singapore, 1994), p. 162.

[17] H. W. Kroto, J. R. Heath, S. C. O'Brien, R. F. Curl, and R. E. Smalley, Nature (London) **318**, 162 (1985).

[18] R. Sachidanandam and A. B. Harris, Phys. Rev. Lett. **67**, 1467 (1991); P. A. Heiney *et al.*, *ibid.*, **67**, 1468 (1991).

[19] A. B. Harris and R. Sachidanandam, Phys. Rev. B **46**, 4944 (1992).

[20] S. Liu, Y. J. Lu, M. M. Kappes, and J. A. Ibers, Science **254**, 408 (1991).

[21] W. I. F. David, R. M. Ibberson, J. C. Matthewman, K. Prassides, T. J. Dennis, J. P. Hare, H. W. Kroto, R. Taylor, and D. R. M. Walton, Nature (London) **353**, 147 (1991).

[22] W. I. F. David, R. M. Ibberson, T. J. S. Dennis, J. P. Hare, and K. Prassides, Europhys. Lett. **18**, 219 (1992).

[23] W. I. F. David, R. M. Ibberson, and T. Matsuo, Proc. R. Soc. London Ser. A **442**, 129 (1993).

[24] R. C. Yu, N. Tea, M. B. Salamon, D. Lorents, and R. Malhotra, Phys. Rev. Lett. **68**, 2050 (1992).

[25] F. Gugenberger, R. Heid, C. Meingast, P. Adelmann, M. Braun, H. Wuhl, M. Haluska, and H. Kuzmany, Phys. Rev. Lett. **69**, 3774 (1992).

[26] T. Matsuo, H. Suga, W. I. F. David, R. M. Ibberson, P. Bernier, A. Zahab, C. Fabre, A. Rassat, and A. Dworkin, Solid State Commun. **83**, 711 (1992).

[27] R. Tycko, G. Dabbagh, R. M. Fleming, R. C. Haddon, A. V. Makhija, and S. M. Zahurak, Phys. Rev. Lett. **67**, 1886 (1991).

[28] R. D. Johnson, C. S. Yannoni, H. C. Dorn, J. R. Salem, and D. S. Bethune, Science **255**, 1235 (1992).

[29] H. A. Ludwig, W. H. Fietz, F. W. Hornung, K. Grube, B. Wagner, and G. J. Burkhart, Z. Phys. B **96**, 179 (1994).

[30] A. Lundin and B. Sundqvist, Europhys. Lett. **27**, 463 (1994).

[31] J. E. Fischer, P. A. Heiney, A. R. McGhie, W. J. Romanow, A. M. Denenstein, J. P. McCauley, Jr., and A. B. Smith III, Science **252**, 1288 (1991).

[32] H. Kataura, N. Irie, N. Kobayashi, Y. Achiba, K. Kikuchi, T. Hanyu, and S. Yamaguchi, Jpn. J. Appl. Phys. **32**, **L** 1667 (1993).

[33] C. Pan, M. P. Sampson, Y. Chai, R. H. Hauge, and J. L. Margrave, J. Phys. Chem. **95**, 2944 (1991).

[34] J. Abrefah, D. R. Olander, M. Balooch, and W. J. Siekhaus, Appl. Phys. Lett. **60**, 1313 (1992).

[35] H. M. James and T. A. Keenan, J. Chem. Phys. **31**, 12 (1959).
[36] P. C. Chow, X. Jiang, G. Reiter, P. Wochner, S. C. Moss, J. D. Axe, J. C. Hanson, R. K. McMullan, R. L. Meng, and C. W. Chu, Phys. Rev. Lett. **69**, 2943 (1992).
[37] L. Pintschovius, B. Renker, F. Gompf, R. Heid, S. L. Chaplot, M. Haluska, and H. Kuzmany, Phys. Rev. Lett. **69**, 2662 (1992).
[38] L. Pintschovius, S. L. Chaplot, R. Heid, M. Haluska, and H. Kuzmany, in *Proceedings of the International Winterschool on Electronic Properties of Novel Materials*, edited by H. Kuzmany, Springer Series in Solid State Science (Springer-Verlag, Berlin, 1993), p. 162.
[39] L. Pintschovius and S. L. Chaplot, Z. Phys. B **98**, 527 (1995).
[40] P. J. Horoyski and M. L. W. Thewalt, Phys. Rev. B **48**, 11 446 (1993).
[41] P. J. Horoyski, M. L. W. Thewalt, and T. R. Anthony, Phys. Rev. B **52**, R6951 (1995).
[42] K. H. Michel, J. R. D. Copley, and D. A. Neumann, Phys. Rev. Lett. **68**, 2929 (1992).
[43] L. C. Biedenharn and J. D. Louck, *Angular Momentum in Quantum Physics* (Addison-Wesley, New York, 1981).
[44] This assumption is based on the argument that for the setting angles of $\approx 22°$ and 86° the electron-poor regions (centers of pentagons or hexagons) of all molecules face the electron-rich regions (''6-6'' bonds) of their nearest neighbors. Indeed, this leads to the minimization of the electrostatic interactions between the valence charge densities. However, this effect is outweighed by the contribution coming from the interaction between the ''core'' charges, so that the total electrostatic interaction is maximized at these setting angles.
[45] R. Heid, Phys. Rev. B **47**, 15 912 (1993).
[46] C. J. Bradley and A. P. Cracknell, *The Mathematical Theory of Symmetry in Solids* (Clarendon, Oxford, 1972).
[47] L. Pintschovius, S. L. Chaplot, G. Roth, M. Haluska, and H. Kuzmany, Phys. Scr. **57**, 102 (1995).
[48] P. Launois, S. Ravy, and R. Moret, Phys. Rev. B **52**, 5414 (1995).
[49] S. Ravy, P. Launois, and R. Moret, Phys. Rev. B **53**, 10 532 (1996).
[50] T. Yildirim and A. B. Harris, Phys. Rev. B **46**, 7878 (1992).
[51] X.-P. Li, J. P. Lu, and R. M. Martin, Phys. Rev. B **46**, 4301 (1992).
[52] D. Klyachko and D. M. Chen, Phys. Rev. Lett. **75**, 3693 (1995).
[53] G. B. M. Vaughan, P. A. Heiney, D. E. Cox, A. R. McGhie, D. R. Jones, R. M. Strongin, M. A. Cichy, and A. B. Smith III, Chem. Phys. **168**, 185 (1992).
[54] A. N. Lommen, P. A. Heiney, G. B. M. Vaughan, P. W. Stephens, D. Liu, D. Li, A. L. Smith, A. R. McGhie, R. M. Strongin, L. Brard, and A. B. Smith III, Phys. Rev. B **49**, 12 572 (1994).
[55] H. Yasuda and T. Yamamoto, Prog. Theor. Phys. **45**, 1458 (1971).